Available online at www.sciencedirect.com
ScienceDirect
Journal of the European Ceramic Society 30 (2010) 2715–2725
www.elsevier.com/locate/jeurceramsoc

Damage law identification of a quasi brittle ceramic from a bending test using Digital Image Correlation

Paul Leplay [a,b,c,*], Julien Réthoré [a], Sylvain Meille [b], Marie-Christine Baietto [a]

[a] Université de Lyon, CNRS INSA-Lyon, LaMCoS UMR 5259, 69621 Villeurbanne, France
[b] Université de Lyon, CNRS INSA-Lyon, MATEIS UMR 5510, 69621 Villeurbanne, France
[c] Saint-Gobain, CREE, 550 av. Alfred Jauffret - BP 224, 84306 Cavaillon, France

Received 7 January 2010; received in revised form 12 May 2010; accepted 20 May 2010
Available online 19 June 2010

Abstract

Although ceramics are generally considered to be elastic brittle solids, some of them are quasi brittle. These ceramics show a non-linear mechanical behaviour resulting most of the time in a difference between their tensile and compressive stress–strain laws. The characterization of their fracture strengths might be biased if linear elastic formulae are used to analyze classical tests like bending tests. Based on Digital Image Correlation (DIC), an efficient technique to measure full field displacements, a methodology is proposed to characterize and model materials with dissymmetric behaviours between tension and compression. Applying specific basis functions for DIC displacement decompositions for bending, compressive and tensile tests, a stress–strain model and its damage law are identified and then validated for aluminium titanate, a damageable micro-cracked ceramic at room temperature. This identification method using DIC can obviously be applied to other quasi brittle materials.

Keywords: Mechanical properties (C); Strength (C); Al_2TiO_5 (D); Digital Image Correlation

1. Introduction

Compared to other materials, ceramics are generally considered to be brittle solids, i.e. with an elastic behaviour followed by an unstable failure. Some of them are quasi brittle and show a non-linear mechanical behaviour. Depending on the occurrence of the non-linearity before or after the maximum load, they are respectively called damageable or strain-softening ceramics. Their quasi brittleness results from the evolution of multiple internal mechanisms. We can mention the most common mechanism and materials, the micro-crack propagation for natural rocks,[1] ceramics made of crystals with anisotropic thermal expansion coefficients,[2,3] refractories,[4] concrete[5] and piezo ceramics.[6] We can also mention other mechanisms like the shear yielding of the fibril interfaces for bones,[7] the crack bridging and the secondary cracking in the frontal process zone for plasters[8] and the transformation toughening for some zirconia.[9]

A dissymmetric evolution of these internal mechanisms might appear between tension and compression, leading to differences of both constitutive laws and fracture strengths for tensile and compressive loadings.

Many efforts have been made to analytically model the relationship between the presence of microstructural defects like cracks and the macroscopic dissymmetry of behaviours and fracture strengths.[10–12] This dissymmetry between tension and compression is also experimentally difficult to quantify. Indeed, bending tests are often preferred in the literature and in the industry to measure fracture strengths, as uniaxial tensile or compressive tests are challenging and costly to perform on ceramics. Bending tests are certainly simpler to implement and work satisfyingly but they also present some risks and limitations.[13] For instance, the load–displacement curves of damageable ceramics are usually analyzed in the symmetric linear elastic context.[14] The determination of the fracture strengths might be biased. Therefore extrapolating uniaxial properties from bending test data might lead to significant errors for quasi brittle ceramics.

Obtaining reliable uniaxial results through bending tests is not a new idea[15] but phenomenological approaches combined with inverse methods are usually preferred.[6,16–18] Numerical inverse methods applied to bending tests certainly provide prac-

* Corresponding author at: Université de Lyon, CNRS INSA-Lyon, 18-20, rue des Sciences, LaMCoS UMR 5259, 69621 Villeurbanne, France. Tel.: +33 4 72 43 71 05.
E-mail address: paul.leplay@insa-lyon.fr (P. Leplay).

0955-2219/$ – see front matter © 2010 Elsevier Ltd. All rights reserved.
doi:10.1016/j.jeurceramsoc.2010.05.021

tical evaluations of uniaxial responses. For ceramics, the strain level at failure is as low (about 10^4) as the limit resolution of conventional DIC is reached. Thus, important numerical regularizations, like Tikhonov regularization, may be required because of the possible amplification of strain measurement errors due to the perturbation sensitivity of the inverse method.[18] Besides, these uniaxial curves do not derive from any thermodynamic framework. It is thus preferred in the present paper to describe the behaviour of the studied ceramic using a damage law within an appropriate thermodynamic framework.

Special care must be taken on strain measurement during bending tests because of the dissymmetry between tension and compression for damageable ceramics. The traditional way is to use gauges or extensometers in order to measure strains on the bent beam.[4,7,18] Digital Image Correlation (DIC) is preferred here since it offers the capacity to access the full displacement field on the whole sample surface instead of only an averaged strain at some pre-defined location.[19,20] This technique based on the optical flow conservation enables the identification of elastic properties.[21] The decomposition adopted for the searched displacement field is a key step for an accurate and reliable displacement measurement. The *a priori* basis function choice is primary to incorporate into the measurement problem mechanical hypotheses.[22] Specific decomposition function sets have already been proposed to extract mechanical quantities from a specific mechanical problem like Brazilian disk, bending or crack propagation tests.[21,23–25] Two new specific function sets for four-point bending and uniaxial tests are proposed in this paper, enabling accurate small strain measurements.

To summarize, the aim of the methodology proposed in this work is to develop new specific decomposition functions for DIC adapted for bending and uniaxial tests (Section 2) in order to identify compressive and tensile constitutive laws and fracture strengths for damageable ceramics (Sections 3 and 4). This methodology is illustrated through an application on aluminium titanate, a micro-cracked ceramic whose mechanical and fracture behaviours have been rather little investigated in literature to the authors' knowledge.

2. Digital Image Correlation developments

2.1. General principle: optical flow conservation

DIC is a full field measurement method which enables one to capture both local and global variations of the displacement of a structure. It is based on the grey level conservation principle between two images of a same structure. Let us call f the reference image, g the deformed image, u the displacement field, b the noise. This technique consists in comparing two successive images to find the displacement field thanks to the optical flow conservation for each pixel of coordinate x:

$$f(x) = g(x + u(x)) - b(x) \tag{1}$$

To determine v, the best approximation possible for u assuming no noise, one can solve this ill-posed inverse problem on chosen regions Ω by minimizing the global error thanks to the functional ϕ:

$$\phi^2(x) = \int\int_{\Omega} [f(x) - g(x + v(x))]^2 \mathrm{d}x \tag{2}$$

The displacement field is decomposed as a linear combination of basis functions N_i:

$$v(x) = \sum_i \alpha_i N_i(x) \tag{3}$$

Using a first order Taylor expansion, the functional ϕ^2 becomes a quadratic form of amplitude increments $d\alpha_i$. Its minimization leads to a linear system written in a matrix form:

$$\left[\int\int_{\Omega} (\nabla g(x + v).N_j(x))(\nabla g(x + v).N_i(x))\,\mathrm{d}x\right]\,\mathrm{d}\alpha_i = \int\int_{\Omega} f(x) - g(x + v)(\nabla g(x + v).N_j(x))\,\mathrm{d}x \tag{4}$$

$$\Leftrightarrow M_{ji}.\mathrm{d}\alpha_i = b_j \tag{5}$$

Once the convergence of amplitude increments $d\alpha_i$ is achieved, the approximated displacement field v is reconstructed on Ω. The final error between u and v is obtained by comparing the real reference image f to a corrected deformed image calculated from the deformed image g and the displacement approximation v:

$$\text{error} = g(x + v(x)) - f(x) \tag{6}$$

The displacement field decomposition in Eq. (3) is one of the key tools of DIC. First, it makes feasible to transform an ill-posed inverse problem into a linear system. Second, it enables one to introduce mechanical hypotheses into a numerical problem leading to a regularization of the displacement solution v. Following this concept, specific basis function sets have already been proposed in the literature: Besnard et al. for arbitrary mechanical problem with bi-linear Q4 elements,[22] Hild et al. for cantilever beam kinematics with a linear curvature element,[23] Roux et al. for stress intensity factor measurements,[24] Réthoré et al. for beam kinematics with NURBS functions.[25] Two new sets of specific functions are now proposed for two particular cases: four-point bending tests with a constant curvature element (Section 2.2) and uniaxial tests with a homogeneous strain element (Section 2.3).

2.2. Particular case: four-point bending kinematics

The four-point bending test is often used in the scientific literature and the industry to characterize the material strengths, as it requires simple sample geometry and equipment. Compared to the three-point bending test, the volume of loaded material is more important leading to more reliable brittle fracture properties. Assuming the Euler–Bernoulli hypotheses for the four-point bending test, the whole kinematics of the central part can be described with the curvature value and the boundary conditions, because the applied moment is constant.

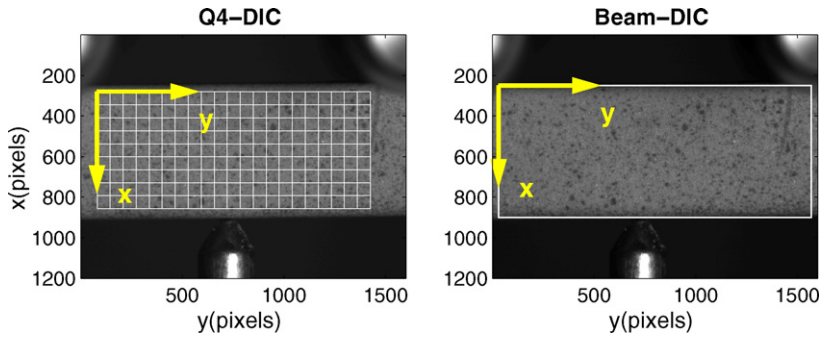

Fig. 1. Reference images and zones of interest for four-point bending tests. Pixel physical size = 10.9 μm.

Some optical approaches have already been used in literature to measure strains during bending tests.[26,27] They are nevertheless limited by their incapacity either to detect rigid-body rotations and translations or to capture full fields for large strains.

The bi-linear Q4-DIC approach developed by Besnard et al.[22] could also be used for the four-point bending test since it is suitable for all mechanical problems with a continuous displacement field. But two drawbacks have to be underlined. First, the noise sensitivity of this general technique may be too important, especially when the strains are very small like for ceramics (see Section 4.1). Second, it is not optimal to average *a posteriori* the displacement over the beam, since there is no direct access to the curvature due to the vanishing of the second order derivatives of the bi-linear Q4 element.

The basis functions for beam bending developed by Hild et al.[23] enables the direct measurement of a beam curvature assumed to be linear over the beam length. This technique is certainly suitable for cantilever beam experiments but not for four-point bending tests.

Therefore developing a specific DIC technique which enables the direct measurement of the constant curvature of a beam is a more efficient approach. This goal can be reached thanks to the *a priori* choice of basis functions for an element with constant second order spatial derivatives.

For a four-point bending test, the displacement field is expressed according to Eq. (3) as a sum of five degrees of freedom (dof) within the region of interest Ω (Fig. 1):

- Assuming a constant beam curvature, three coefficients (dof: γ_0,θ_0 and v_{x0}) are required for a two-degree polynomial describing the beam deflection v_x:

$$\frac{\partial^2 v_x(x,\,y)}{\partial y^2} = \gamma_0 \tag{7}$$

$$\frac{\partial v_x(y)}{\partial y} = \gamma_0 y + \theta_0 \tag{8}$$

$$v_x(y) = \frac{\gamma_0}{2} y^2 + \theta_0 y + v_{x0} \tag{9}$$

  For an Euler–Bernoulli kinematics, the corresponding horizontal displacement v_y is:

$$v_y(x,\,y) = -x\frac{\partial v_x(y)}{\partial y} = -x(\gamma_0 y + \theta_0) \tag{10}$$

- Horizontal strain and displacement (dof: v_{y0} and ϵ_{yy}) are introduced to accommodate test imperfections:

$$v_y(y) = v_{y0} + y\epsilon_{yy} \tag{11}$$

  The vertical location of the neutral axis is not a parameter of this formulation. In fact, Eqs. (7)–(10) determine its location at the mid-height of the beam section. Eq. (11) adds a possible homogeneous strain. A vertical shift of the zero strain axis is thus allowed.

Finally, Eq. (3) becomes for a four-point bending test kinematics:

$$\begin{bmatrix} v_x \\ v_y \end{bmatrix} = \begin{bmatrix} 0.5y^2 & y & 1 & 0 & 0 \\ -xy & -x & 0 & 1 & y \end{bmatrix} \cdot \begin{bmatrix} \gamma_0 \\ \theta_0 \\ v_{x0} \\ v_{y0} \\ \epsilon_{yy} \end{bmatrix} \tag{12}$$

This specific decomposition being included in matrix system (5), the axial strain becomes directly available with a high accuracy because it is a linear function of the vertical coordinates x, γ_0, θ_0 and ϵ_{yy}. An artificial displacement field is applied in order to test the *a priori* performance of the proposed basis functions. With translations of amplitudes from 0 to 1 pixel in y direction, displacement and strain accuracies respectively are 3.2×10^{-5} pixel and 5.0×10^{-8} (for the region Ω of the image used in Section 4.1). The mean DIC error is equal to 0.04% of the dynamic of the image. The approach developed in this section will henceforth be called 'beam-DIC'.

2.3. Particular case: uniaxial tensile and compressive kinematics

Even if uniaxial tests are more complicated to implement and run than bending tests, they provide direct informations on the material properties. To measure displacement and strain fields during such uniaxial tests, the Q4-DIC approach could again be used but similar drawbacks as encountered for bending tests appear. DIC global formulation allowing displacement decomposition with arbitrary basis functions, it is again preferred to use specific functions adapted to the test kinematics instead of averaging *a posteriori* the displacement field in order to extract the searched mechanical quantities (Fig. 2).

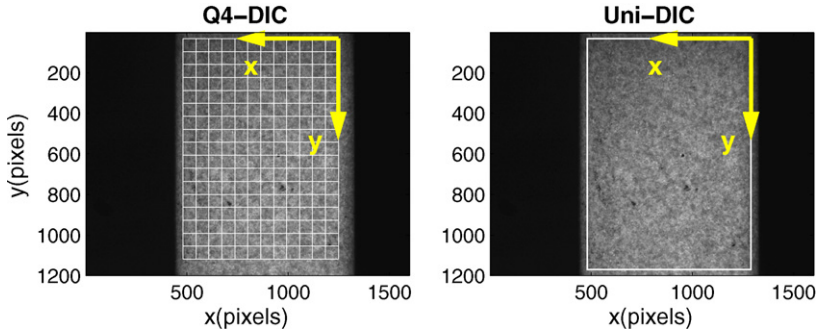

Fig. 2. Reference images and zones of interest for uniaxial tests. Pixel physical size = 10.9 μm.

Tensile or compressive tests displacement kinematics can be expressed according to six degrees of freedom:

- Assuming homogeneous strain on the sample surface, three parameters are necessary for vertical and horizontal strains (dof: ϵ_{xx} and ϵ_{yy}) and one for the shear strain (dof: ϵ_{xy}) to describe the kinematics within Ω region. One can note that if the material Poisson's ratio was already known, one of the two degrees of freedom ϵ_{xx} or ϵ_{yy} would have been useless.

$$v_x(x) = x\epsilon_{xx} + \frac{y}{2}\epsilon_{xy} \tag{13}$$

$$v_y(y) = y\epsilon_{yy} + \frac{x}{2}\epsilon_{xy} \tag{14}$$

- To accommodate test imperfections, three degrees of freedom are added for the description of the vertical and horizontal translations (dof: v_{x0} and v_{y0}) and for in-plane rotation (dof: θ_{xy}).

$$v_x(y) = v_{x0} + y\theta_{xy} \tag{15}$$

$$v_y(x) = v_{y0} - x\theta_{xy} \tag{16}$$

Eq. (3) finally becomes for an uniaxial test kinematics:

$$\begin{bmatrix} v_x \\ v_y \end{bmatrix} = \begin{bmatrix} x & 0 & 0.5y & y & 1 & 0 \\ 0 & y & 0.5x & -x & 0 & 1 \end{bmatrix} \cdot \begin{bmatrix} \epsilon_{xx} \\ \epsilon_{yy} \\ \epsilon_{xy} \\ \theta_{xy} \\ v_{0x} \\ v_{0y} \end{bmatrix} \tag{17}$$

This specific decomposition enables a direct access to the homogeneous strain value for compressive or tensile tests without cumbersome averaging post-processing. For translations of amplitudes from 0 to 1 pixel in x and y directions, displacement and strain accuracies respectively are 1.1×10^{-4} pixel and 1.3×10^{-7} (for the regions Ω of the images used in Sections 4.2 and 4.3). The mean DIC error is equal to 0.1% of the dynamic of the image. The approach developed in this section will henceforth be called 'uni-DIC'.

Specific functions for DIC being proposed, bending and uniaxial tests are run to identify mechanical properties of damageable ceramics.

3. Experimental procedure

3.1. Aluminium titanate

Aluminium titanate Al_2TiO_5 is a micro-cracked ceramic due to the anisotropic thermal expansion coefficient of its crystals.[3] The micro-cracks appear at grain boundaries during cooling from the sintering temperature. This is due to the thermal expansion mismatch between crystals. Since closing and healing of these micro-cracks occur during later heatings, aluminium titanate has a low thermal expansion exhibiting consequently an excellent thermal shock resistance.[28,29] Secondary phases such as MgO, ZrO_2, SiO_2 or ZrO_2 are often used to stabilize at high temperature and strengthen pure aluminium titanate.[30] This quasi brittle material becomes an excellent potential ceramic for industrial thermostructural applications like, for instance, in the automotive industry with catalyst carriers, thermal insulation liners and gas filters.[31]

The relationship between the sintering process, the microstructure, the secondary silicate phase and the final thermal expansion coefficient has been widely studied[28–30,32] but mechanical and fracture aspects are rare in literature.[33–35] Aluminium titanate is however known to have a damageable mechanical behaviour due to the micro-crack propagation.[34]

3.2. Samples and mechanical tests

The tested material is mainly made of aluminium titanate with a secondary silicate phase. It exhibits a high porosity volume fraction varying from 40 to 50%. The samples were extruded then sintered for a final rectangular section of $B \times W = 5.1 \times 7.3\,mm^2$. Five samples were used for each mechanical test conducted at room temperature.

- Four-point bending tests were performed on a hydraulic machine (Instron 8502) with a 5000 N load cell. The lower span was $D_1 = 60$ mm and the upper span $D_2 = 20$ mm. A linear variable differential transducer (LVDT) was used to control the deflection at the middle of the beam at a rate of 0.05 mm/min. Rubber bands have been used to fasten the rollers to the main fixtures (Fig. 1).

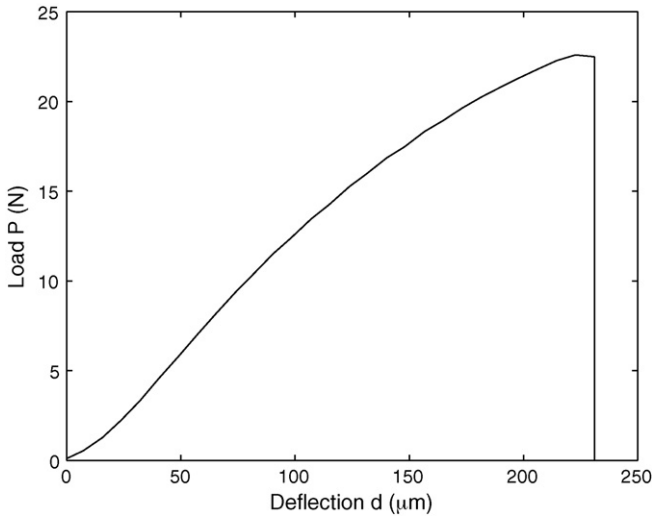

Fig. 3. Experimental load–deflection curve for one of the four-point bending tests on aluminium titanate. Room temperature.

- Compressive tests were carried out using the same hydraulic machine, load cell and crosshead speed. The sample length was about 25 mm.
- Tensile tests were realized on an electromechanical machine (Instron 1195) with a 500 N load cell and a 0.02 mm/min elongation speed. The samples were about 20 mm long. They were stuck to the fixtures thanks to a slow-setting glue likely to penetrate into the material pores. A special care for the vertical alignment between the samples and the machine was taken thanks to two cardan joints.

3.3. Optical equipment

A CCD camera has been used to continuously visualize the sample surface during each mechanical test. The maximum image resolution of this camera is 1200 × 1600 pixels with an 8-bit digitization for grey levels. The acquisition frequency was one image every five seconds. A painted random pattern was spread on the sample surface to enhance the image contrast.

The optical magnification of classical lenses depending on the distance to the sample surface, out-of-plane displacements or misalignments might induce artificial magnifications interpreted as in-plane strains by the DIC system. To overcome this possible error, the CCD camera was fitted with a 200 mm telecentric lens, ensuring a magnification independent on the distance. Each pixel has here a 10.9 μm physical size.

4. Results for aluminium titanate

4.1. Four-point bending test

Fig. 3 shows a non-linear load–deflection curve. For the five samples, the averaged maximum load P_{max} is 22.7 ± 0.4 N for a 208 ± 22 μm vertical deflection d at the middle of the beam. Since ceramics are known to break at low strains,[31] one may use linear elastic formulae (18) and (19) to analyze this four-point bending test[36]:

$$\epsilon_{elastic} = \frac{12dW}{2D_1^2 + 2D_1D_2 - D_2^2} \quad (18)$$

$$\sigma_{elastic} = \frac{3P(D_1 - D_2)}{2BW^2} \quad (19)$$

where P is the applied load, d is the vertical deflection at the beam middle, W is the height, B is the width, D_1 and D_2 are the lower and upper spans.

These elastic formulae lead to a fracture strength of 5.0 ± 0.1 MPa and a failure strain of 0.19 ± 0.1%. But two problems have to be underlined. First, formula (18) does not take into account the influence of the shear loading on the global beam deflection d.[36] This might lead to a significant overestimation of the axial strain ϵ (+4% with our geometrical configuration). Second, these elastic formulae implicitly assume a symmetry between tension and compression—i.e. a neutral axis located at the mid-height of the beam section.

This elastic approach is widely adopted in the literature and in the industry to characterize aluminium titanate at room temperature or at high temperature.[33,37,38] Only Liu and Perera used a different Eq. (20) to calculate the 'true' fracture strength of two aluminium titanate ceramics containing magnesium and iron[39]:

$$\sigma_{`true'} = \frac{(D_1 - D_2)}{BW^2}\left(P + \frac{d}{2}\frac{\partial P}{\partial d}\right) \quad (20)$$

Although this formula is better suited for inelastic materials, it is also based on the assumption of a symmetric tensile and compressive behaviour.[40] A 'true' fracture strength of 3.9 ± 0.1 MPa is obtained according to Eq. (20), but this value has no physical meaning because of the difference between tensile and compressive mechanical behaviour of the aluminium titanate. Strength values have been also determined with this equation for damageable ceramics like zirconia[41] or synthetic rocks[42] without having validating the assumption of symmetric behaviour.

It is thus not possible to quantify the strength of such damageable ceramics based on the deflection and the load measurements. Therefore one needs to have access the overall strain field during a four-point bending test. The Q4-DIC and beam-DIC approaches are now used to achieve this full field measurement for one of the five samples.

Using the Q4-DIC approach (198 elements/size length = 64 pixels) to measure displacement field amplitudes v_y, the corresponding strain values ϵ_{yy} are not reliable (Fig. 4). It is hence impossible to determine accurately the exact neutral axis location. Using the beam-DIC approach (Section 2.2) with one element, the measured displacement field v_y and the corresponding axial strain field ϵ_{yy} are more regular and accurate (Fig. 5). Even if the zone of interest Ω is wider for the beam-DIC approach (Fig. 1), the ratio between inputs (grey level pixels) and outputs (degrees of freedom) per element is higher than those obtained according to the Q4-DIC approach. Therefore the algorithm convergence is twice faster, the approximated solution is more accurate and the post-processing is simpler.

The axial strain field measured during the bending test reveals a dissymmetric tensile-compressive behaviour (Fig. 5). Indeed,

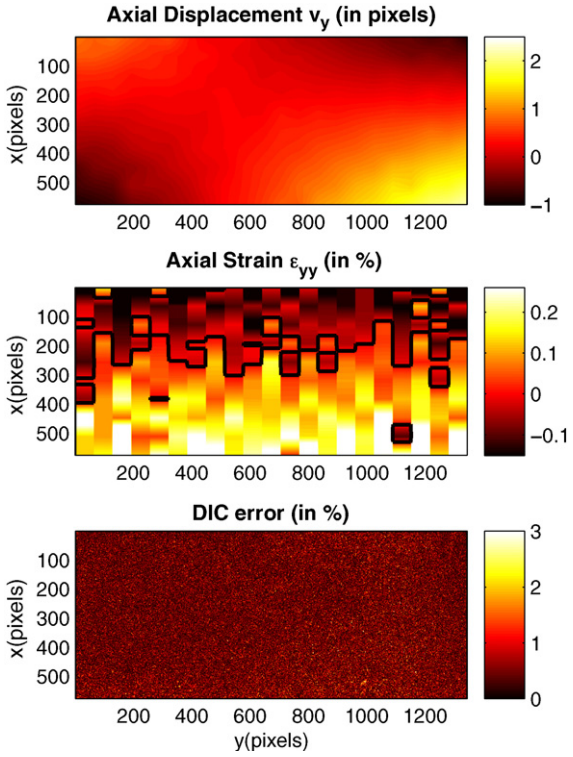

Fig. 4. Kinematics measured using the Q4-DIC approach just before failure for the bending test. The black line is ϵ_{yy} iso-0.

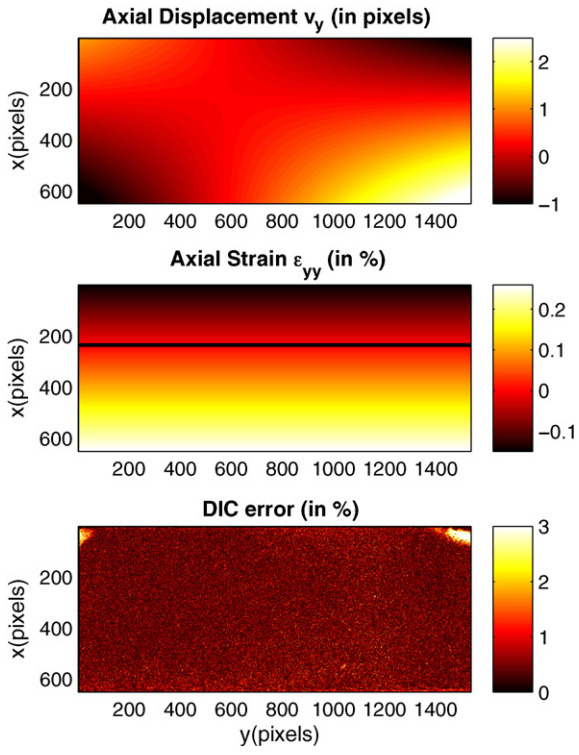

Fig. 5. Kinematics measured using the beam-DIC approach just before failure for the bending test. The black line is ϵ_{yy} iso-0.

the neutral axis translates progressively as the test increases toward the compressive part of the beam. At the failure load, the beam-DIC approach respectively yields to maximum strains of $+0.26\%$ and -0.15% for tensile and compressive parts. This neutral axis shift during the test indicates a difference between compressive and tensile behaviours that was previously not taken into account in Eqs. (18)–(20).

During the bending test, the correlation error calculated according to Eq. (6) is homogeneous and the mean error remains between 0.5 and 0.6% (Fig. 5). This low error value confirms that the kinematics hypotheses of the beam-DIC approach are consistent. Besides, this homogeneous error value reveals that there is no visible damage localization until a catastrophic failure of the aluminium titanate sample occurs. The important error at the top corners of the image corresponds merely to the two rubber bands used to fasten the two rollers to the upper fixture. It has been checked on several images that the kinematics obtained using the beam-DIC approach lead to a deflection in a very good agreement with the value measured using the LVDT at the middle of the beam, enforcing the quality of the kinematics measurement. Finally, some tensile and compressive tests must be carried out to get a deeper material characterization due to the dissymmetry observed during the four-point bending test. Instead of performing a phenomenological approach combined with an inverse method to identify uniaxial behaviours, it has been preferred to determine thermodynamically admissible models from experimental compressive (Section 4.2) and tensile (Section 4.3) test data.

4.2. Uniaxial compressive test

Even if the Q4-DIC approach (204 elements/size length = 64 pixels) allows one to identify the axial and shear displacement fields on the sample surface, it is impossible to obtain a reliable value for the axial strain (Fig. 6). On the contrary, the uni-DIC approach (Section 2.3) leads directly to a homogeneous strain value (Fig. 7). The axial strain at failure is $-0.74 \pm 0.03\%$ for a maximum stress of 27.5 ± 1.1 MPa.

The stress–strain curve (Fig. 8) shows that the mechanical behaviour is linear elastic until a strain of $-0.50 \pm 0.05\%$ is reached. The secant modulus remains almost equal to 4.6 until this strain limit. Oscillations of the secant modulus curve are observed for strains ranging from 0.0 to -0.03% due to a lack of accuracy in both the strain and load measurements. When strains vary from -0.50 to -0.74%, the progressive DIC error increasing indicates that the strain is no more homogeneous everywhere at the sample surface. In fact, strain begins to localize at one of the sample corners where an unstable crack will appear before the failure. For aluminium titanate tested in compression, the failure shows a very limited strain-softening behaviour.

Strains have been quantified according to the beam-DIC approach during the four-point bending test in Section 4.1. The value of -0.15% was reached in the compressive part of the beam just before the catastrophic failure. It means that the mechanical behaviour for the compressive part of the bent beam can be considered as linear elastic with a Young modulus of 4.6 GPa.

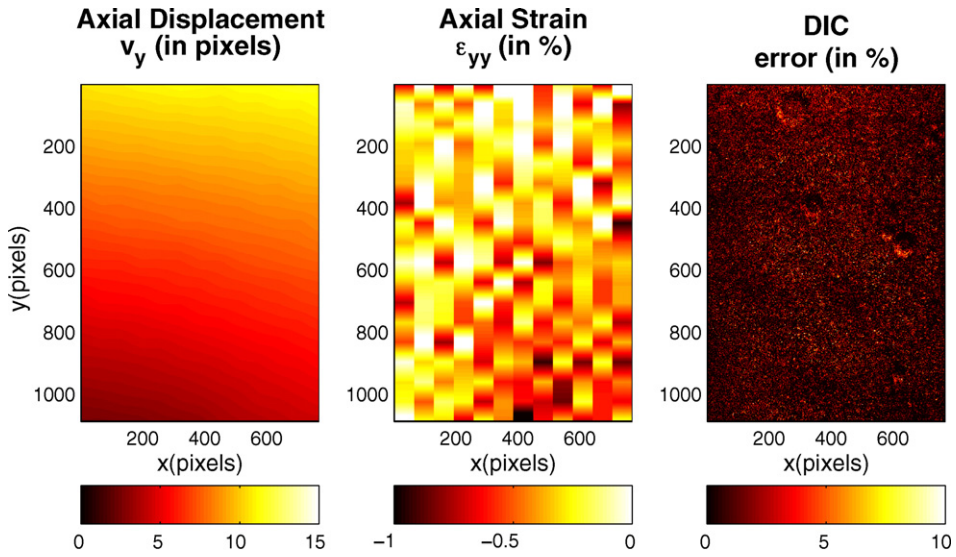

Fig. 6. Kinematics measured using the Q4-DIC approach for the maximum load in the elastic domain for the compressive test.

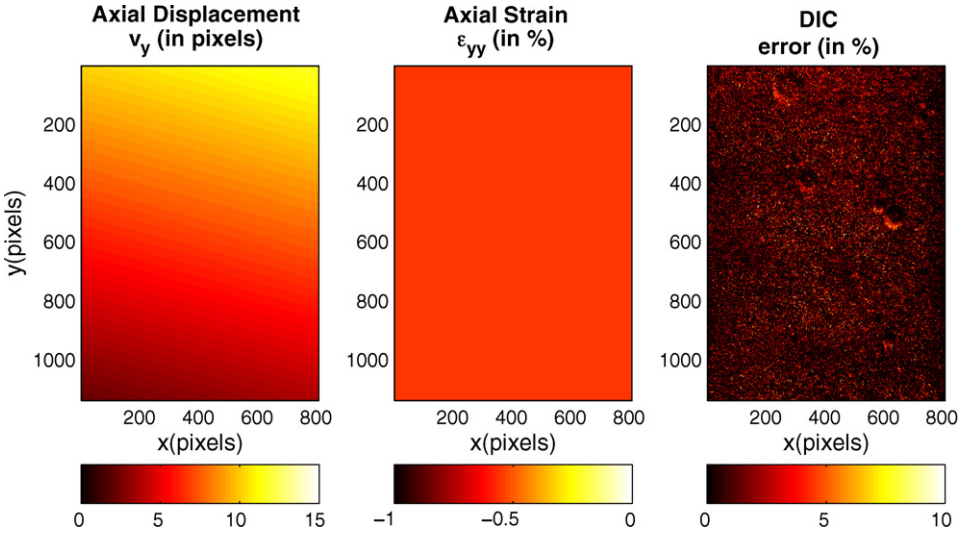

Fig. 7. Kinematics measured using the uni-DIC approach for the maximum load in the elastic domain for the compressive test.

4.3. Uniaxial tensile test

The measured maximum stress is equal to 3.0 ± 0.3 MPa for an axial strain of $+0.11 \pm 0.05\%$ using the uni-DIC approach (Section 2.3). The stress–strain curve is not linear and the secant modulus descreases progressively from 4.7 to 2.7 GPa when the axial strain increases (Fig. 9). Oscillations of the secant modulus curve are observed when for strains ranging to 0.00 to $+0.01\%$ because of the insufficient accuracy of strain and load measurements, as obtained for the compressive test. The initial modulus is almost equal to the one measured in compression. This damageable behaviour is linked to the progressive propagation of the micro-cracks of the aluminium titanate. Since the mean error is low and almost constant, it means that the strain field is really homogeneous without visible damage localization in the sample surface until catastrophic failure.

Failure always occurs close to the glue interface at one of the sample extremities. But it has to be highlighted that the fracture surfaces were clean (i.e. without glue) so that the obtained results do characterize the porous ceramic.

Maximum ϵ_{yy} strain is equal to +0.11% in the tensile test whereas values of +0.26% have been measured during the four-point bending test. Such results have already been observed in the literature.[16,43] From the bending tests, the Weibull modulus have been roughly estimated to be higher than 40. A difference of sample size cannot totally explain this difference of failure strains. Two assumptions can be put forth to explain why smaller strain values are reached during an uniaxial test rather than during the previous bending one. First, the rigidity increases at the interface due to the glue, leading surely to a stress concentration in this region. Higher strains might be reached for a tensile test with a better boundary condition control. Second, a structural effect may be taken into account between two different tests[43]: whereas the crack propagation is quickly unstable during a tensile test, the cracking in the outer layer of a bent beam is forced to remain distributed because of the constraint provided by the

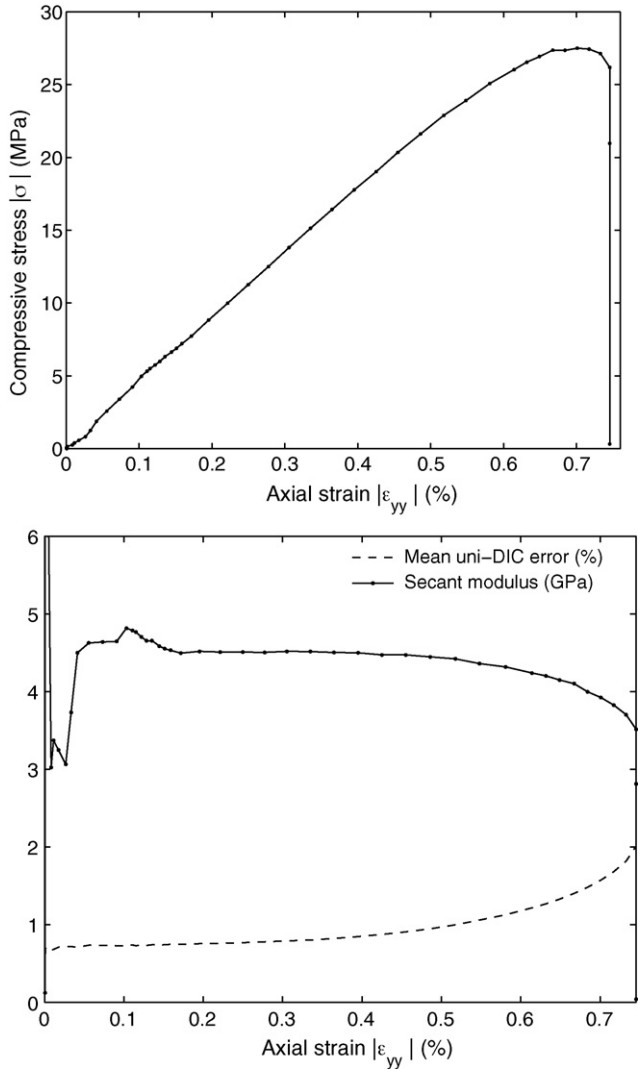

Fig. 8. Results obtained using the uni-DIC approach for the compressive test on aluminium titanate.

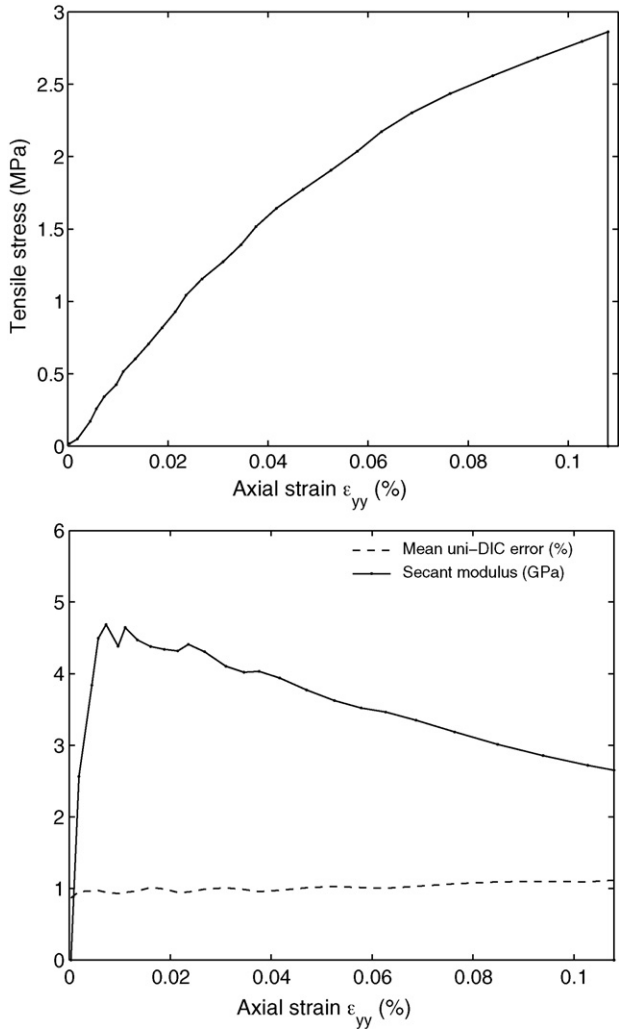

Fig. 9. Results obtained using the uni-DIC approach for the tensile test on aluminium titanate.

uncracked compressive zone: higher strains can thus be reached before failure. The transition from stability to instability depends on the whole stress field of the considered structure. Such structural size effects in bending tests have also been highligthed for mechanisms of crack propagation for other highly porous materials like plaster.[8]

4.4. Prediction of the bending curve through a mechanical model

The aim of this last section is to identify a stress–strain model which can be used henceforth, for instance, in a finite element simulation. The model validation is achieved by predicting the experimental load during a four-point bending test at room temperature. It has been shown that the mechanical behaviour is elastic for strains from 0.0 to −0.5% (Section 4.2). The lowest compressive strains measured using the beam-DIC approach being −0.15%, an elastic law is well suited to describe the compressive behaviour during a bending test:

$$\sigma_{\text{compression}}(\epsilon) = E_0\epsilon \tag{21}$$

It has been shown that the mechanical behaviour is damageable in tension (Section 4.3). The fracture strain measured using the uni-DIC approach was +0.11% during the tensile test, whereas strains of +0.26% obtained using the beam-DIC approach were reached during the bending test. To overcome this lack of experimental data between +0.11 and +0.25%, a damage law is proposed to describe the tensile behaviour. The micro-crack propagation law is represented by an exponential function $D(\epsilon)$ with two new parameters a and b. Such exponential damage laws have already been observed on other quasi brittle ceramics.[44] The same modulus E_0 is used in order to impose a modulus continuity between tensile and compressive laws. This modulus continuity has been experimentally observed in uniaxial tests (4.6 GPa in compression and 4.7 GPa in tension).

$$D_{\text{tension}}(\epsilon) = a\left(1 - \exp\left(-\frac{\epsilon}{b}\right)\right) \tag{22}$$

$$\sigma_{\text{tension}}(\epsilon) = E_0(1 - D(\epsilon))\epsilon \tag{23}$$

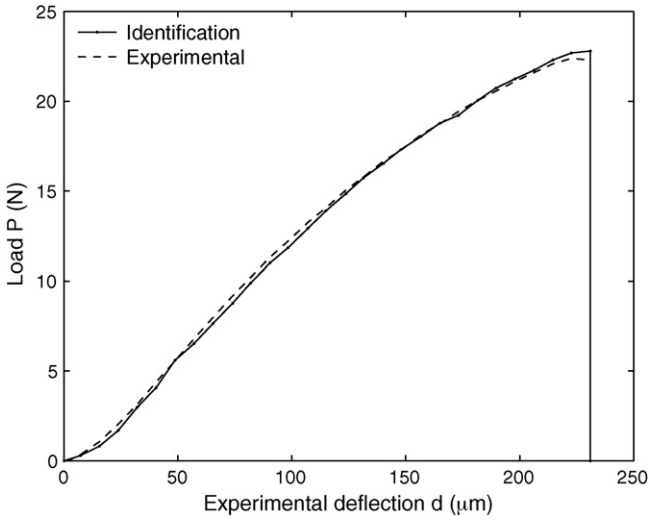

Fig. 10. Comparison between the identified and experimental applied loads for the bending test.

To identify the numerical values of the three parameters (E_0, a, b), the load applied during the four-point bending test is quantified according to the previous constitutive laws. For every pixel of coordinate x, the strain is measured using the beam-DIC approach and the corresponding stress is calculated using Eqs. (21)–(23). There are some pixels which correspond to the beam but are just above or below the DIC zone of interest. Knowing W, the actual height of the section, the strain field has been linearly extrapolated for these few pixels not included in the zone of interest. Then, the load P is calculated on the beam section by integrating the moment with respect to the neutral axis location n:

$$P = \frac{4B}{D_1 - D_2} \int_{-W/2}^{+W/2} \sigma(\epsilon(x))(x - n)\,\mathrm{d}x \tag{24}$$

A Levenberg–Marquardt algorithm has been used to solve this inverse problem to identify the values (E_0, a, b) from the load measurements. Fig. 10 presents a load–deflection curve with the parameter values: $E_0 = 4.67$ GPa, $a = 0.874$ and $b = 0.00136$ (Fig. 11). The load values come from either the load cell or the identified constitutive laws applied to the strain fields measured using the beam-DIC approach. The deflection values come here from the LVDT. The simulated load curve fits well the experimental data.

It has been checked that the E_0 value is consistent with uniaxial test data and with an ultrasonic measurement which led to an Young's modulus of 4.69 ± 0.15 GPa. Finally, it has been checked that these constitutive laws lead for a bending test to the same neutral axis location than the beam-DIC approach on Fig. 5.

These elastic and damageable laws for aluminium titanate are thermodynamically admissible.[14] Thus they can be used directly in a finite-element numerical simulation.

Whereas linear elastic formulae gave fracture strengths of ±5.0 MPa in tension and in compression, the identified constitutive law leads to a strength of +3.5 MPa for tension and a stress of −7.1 MPa for compression at failure (Fig. 12). Relative errors

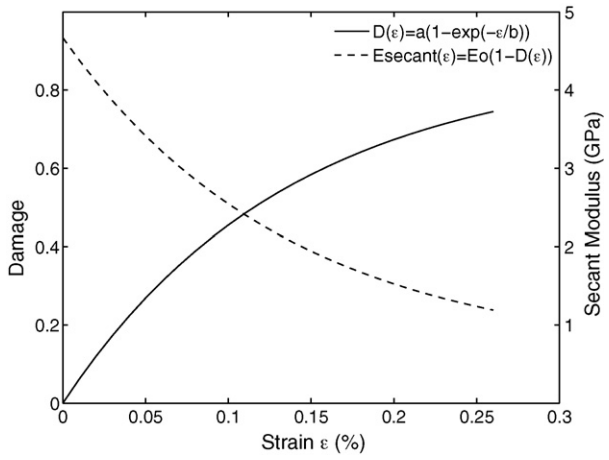

Fig. 11. Damage law accounting for micro-crack propagation for aluminium titanate under a tensile loading.

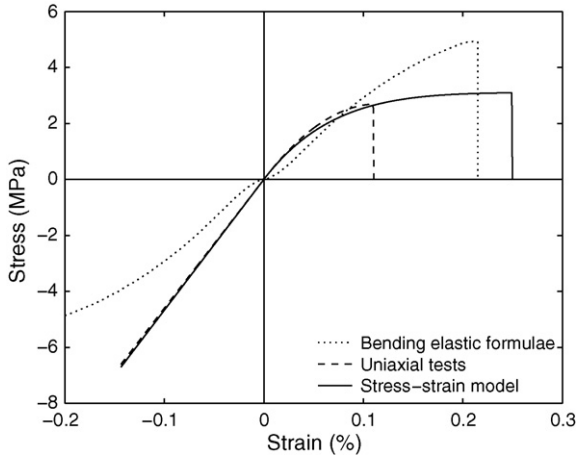

Fig. 12. Measured and identified stress–strain curves for aluminium titanate.

of 30–40% were thus done according to the elastic formulae. Furthermore, the damageable behaviour of aluminium titanate observed during the bending test is only dictated by the micro-crack propagation in the tensile part. Finally, the catastrophic failure of the bent beam without visible damage localization results also from the tensile behaviour.

5. Conclusion

Linear elastic formulae must not be used to analyze mechanical tests performed on quasi brittle ceramics, otherwise significant errors might be made concerning the identification of fracture strengths. Therefore a methodology based on Digital Image Correlation (DIC) has been proposed to characterize damageable ceramics which have different mechanical behaviours under tensile and compressive loadings.

DIC is an efficient optical technique for full field strain measurements, especially when associated with a specific displacement decomposition. It enables one to introduce mechanical hypotheses into the measurement problem. Two specific basis functions have been developed: a constant curvature element for four-point bending tests (beam-DIC approach)

and a homogeneous strain element for uniaxial tests (uni-DIC approach). Two main advantages about using specific decompositions have to be reminded. First, the searched mechanical quantities are easily extractable since they are directly among the degrees of freedom of the system. Second, the obtained results are less sensitive to noise, so very small strains can be measured. This last point is very important for the characterization of ceramics.

The specific tools developed for DIC have been applied to aluminium titanate at room temperature. During a four-point bending test, the non-centered neutral axis location indicated a difference between tension and compression. Uniaxial tests revealed that the mechanical behaviour can be considered as elastic in compression and as damageable in tension. The non-linear behaviour and the catastrophic failure of bending tests result exclusively from the micro-crack propagation inside the tensile part of the bent beam. Then a mechanical stress–strain model and its damage law have been identified and validated by successfully predicting the load curve of the four-point bending test. A difference of 30–40% was observed for fracture strengths between the identified constitutive laws and the linear elastic formulae.

This methodology brings a new alternative to characterize quasi brittle ceramics instead of using conventional linear formulae based on assumptions not always valid. In addition to its simplicity, it allows a direct identification of uniaxial stress–strain models from a classical bending test. This methodology has been applied in this paper to aluminium titanate. Obviously, it can be applied to other quasi brittle materials among biomaterials, cements, plasters, concrete, composites, rocks and porous ceramics.

Acknowledgments

This work is financially supported by the ANRT through the contract no. 2008/501. The authors wish to thank Fabiano Rodrigues and his colleagues at the CREE (Saint-Gobain group) for providing the samples and also supporting this research project.

References

[1]. Kachanov ML. Microcrack model of rock inelasticity. Part II. Propagation of microcracks. *Mechanics of Materials* 1982;**1**(1):29–41.

[2]. Swain MV. Quasi-brittle behaviour of ceramics and its relevance for thermal shock. *Engineering Fracture Mechanics* 1991;**40**(4–5):871–7.

[3]. Thomas HAJ, Stevens R. Aluminium titanate: a literature review. I. Microcracking phenomena. *British Ceramic Transactions Journal* 1989;**88**(4):144–51.

[4]. Simonin F, Olagnon C, Maximilien S, Fantozzi G, Diaz LA, Torrecillas R. Thermomechanical behavior of high-alumina refractory castables with synthetic spinel additions. *Journal of the American Ceramic Society* 2000;**83**(10):2481–90.

[5]. Shah SP, Sankar R. Internal cracking and strain softening response of concrete under uniaxial compression. *ACI Materials Journal* 1987;**84**(3):200–12.

[6]. Fett T, Munz D, Thun G. Nonsymmetric deformation behavior of lead zirconate titanate determined in bending tests. *Journal of the American Ceramic Society* 2005;**81**(1):269–72.

[7]. Mercer C, He MY, Wang R, Evans AG. Mechanisms governing the inelastic deformation of cortical bone and application to trabecular bone. *Acta Biomaterialia* 2006;**2**(1):59–68.

[8]. Meille S, Saadaoui M, Reynaud P, Fantozzi G. Mechanisms of crack propagation in dry plaster. *Journal of the European Ceramic Society* 2003;**23**(16):3105–12.

[9]. Rauchs G, Fett T, Munz D. R-curve behaviour of 9ce-tzp zirconia ceramics. *Engineering Fracture Mechanics* 2002;**69**(3):389–401.

[10]. Kachanov M. Effective elastic properties of cracked solids: critical review of some basic concepts. *Applied Mechanics Reviews* 1992;**45**:304.

[11]. Dragon A, Halm D, Désoyer T. Anisotropic damage in quasi-brittle solids: modelling, computational issues and applications. *Computer Methods in Applied Mechanics and Engineering* 2000;**183**(3–4):331–52.

[12]. Gambarotta L, Lagomarsino S. A microcrack damage model for brittle materials. *International Journal of Solids and Structures* 1992;**30**(2):177–98.

[13]. Quinn GD, Morrell R. Design data for engineering ceramics: a review of the flexure test. *Journal of the American Ceramic Society* 1991;**74**(9):2037–66.

[14]. Lemaitre J, Chaboche JL. *Mécanique des Materiaux Solides*. 2nd ed. Paris: Dunod; 1988.

[15]. Nádai A. *Plasticity*. New York: McGraw-Hill; 1931.

[16]. Laws V. Derivation of the tensile stress–strain curve from bending data. *Journal of Materials Science* 1981;**16**(5):1299–304.

[17]. Mayville RA, Finnie I. Uniaxial stress–strain curves from a bending test. *Experimental Mechanics* 1982;**22**(6):197–201.

[18]. Schajer GS, An Y. Inverse calculation of uniaxial stress–strain curves from bending test data. *Journal of Engineering Materials and Technology* 2009;**131**:041001.

[19]. Sutton MA, Wolters WJ, Peters WH, Ranson WF, McNeill SR. Determination of displacements using an improved digital correlation method. *Image and Vision Computing* 1983;**1**(3):133–9.

[20]. Chu TC, Ranson WF, Sutton MA. Applications of digital-image-correlation techniques to experimental mechanics. *Experimental Mechanics* 1985;**25**(3):232–44.

[21]. Hild F, Roux S. Digital image correlation: from displacement measurement to identification of elastic properties—a review. *Strain* 2006;**42**:69–80.

[22]. Besnard G, Hild F, Roux S. Finite-element displacement fields analysis from digital images: application to portevin–le châtelier bands. *Experimental Mechanics* 2006;**46**(6):789–803.

[23]. Hild F, Roux S, Gras R, Guerrero N, Marante ME, Florez-Lopez J. Displacement measurement technique for beam kinematics. *Optics and Lasers in Engineering* 2009;**47**(3–4):495–503.

[24]. Roux S, Hild F. Stress intensity factor measurements from digital image correlation: post-processing and integrated approaches. *International Journal of Fracture* 2006;**140**(1):141–57.

[25]. Réthoré J, Elguedj T, Simon P, Coret M. On the use of nurbs functions for displacement derivatives measurement by digital image correlation. *Experimental Mechanics* 2009.

[26]. Meuwissen MHH, Oomens CWJ, Baaijens FPT, Petterson R, Janssen JD. Determination of the elasto-plastic properties of aluminium using a mixed numerical–experimental method. *Journal of Materials Processing Technology* 1998;**75**(1):204–11.

[27]. Eberl C, Gianola DS, Hemker KJ. Mechanical characterization of coatings using microbeam bending and digital image correlation techniques. *Experimental Mechanics* 2008:1–13.

[28]. Kim HC, Lee KS, Kweon OS, Aneziris CG, Kim IJ. Crack healing, reopening and thermal expansion behavior of Al_2TiO_5 ceramics at high temperature. *Journal of the European Ceramic Society* 2007;**27**(2–3):1431–4.

[29]. Kim IJ, Gauckler LJ. Excellent thermal shock resistant materials with low thermal expansion coefficients. *Journal of Ceramic Processing Research* 2008;**9**(3):240–5.

[30]. Tsetsekou A. A comparison study of tialite ceramics doped with various oxide materials and tialite–mullite composites: microstructural, thermal and mechanical properties. *Journal of the European Ceramic Society* 2005;**25**(4):335–48.

[31]. Munz D, Fett T. *Ceramics: mechanical properties, failure behaviour, materials selection*. Springer; 1999.

[32]. Giordano L, Viviani M, Bottino C, Buscaglia MT, Buscaglia V, Nanni P. Microstructure and thermal expansion of Al_2TiO_5–$MgTi_2O_5$ solid solutions obtained by reaction sintering. *Journal of the European Ceramic Society* 2002;**22**(11):1811–22.

[33]. Chen CH, Awaji H. Temperature dependence of mechanical properties of aluminum titanate ceramics. *Journal of the European Ceramic Society* 2007;**27**(1):13–8.

[34]. Hamano K, Ohya Y, Nakagawa Z. Crack propagation resistance of aluminium titanate ceramics. *International Journal of High Technology Ceramics* 1985;**1**(2):129–37.

[35]. Melendez-Martinez JJ, Jimenez-Melendo M, Dominguez-Rodriguez A, Wotting G. High temperature mechanical behavior of aluminium titanate–mullite composites. *Journal of the European Ceramic Society* 2001;**21**(1):63–70.

[36]. Timoshenko SP. *Strength of materials. Part I. Elementary theory and problems*. D. Van Nostrana, Inc.; 1930.

[37]. Ohya Y, Nakagawa Z, Hamano K. Crack healing and bending strength of aluminium titanate ceramics at high temperature. *Journal of the American Ceramic Society* 1988;**71**(5):232–3.

[38]. Oikonomou P, Dedeloudis C, Stournaras CJ, Ftikos C. Stabilized tialite–mullite composites with low thermal expansion and high strength for catalytic converters. *Journal of the European Ceramic Society* 2007;**27**(12):3475–82.

[39]. Liu TS, Perera DS. Long-term thermal stability and mechanical properties of aluminium titanate at 1000–1200 °C. *Journal of Materials Science* 1998;**33**(4):995–1001.

[40]. Nádai A. *Theory of flow and fracture of solids*. New York: McGraw-Hill; 1950.

[41]. Gogotsi GA. Mechanical behaviour of yttria- and ferric oxide-doped zirconia at different temperatures. *Ceramics International* 1998;**24**(8): 589–95.

[42]. Latella B, Liu T. High-temperature strength behavior of synroc-c. *Journal of the American Ceramic Society* 2001;**84**(1):117–22.

[43]. Bazant ZP, Li Z. Modulus of rupture: size effect due to fracture initiation in boundary layer. *Journal of Structural Engineering* 1995;**121**(4): 739–46.

[44]. Swain MV. R-curve behavior and thermal shock resistance of ceramics. *Journal of the American Ceramic Society* 1990;**73**(3):621–8.